Optical Bistability and Photon Statistics in Cavity Quantum Electrodynamics

G. Rempe, R. J. Thompson, R. J. Brecha,[a] W. D. Lee,[b] and H. J. Kimble

Norman Bridge Laboratory of Physics 12-33, California Institute of Technology, Pasadena, California 91125
(Received 28 June 1991)

The quantum statistical behavior of a small collection of N two-state atoms strongly coupled to the field of a high-finesse optical cavity is investigated. Input-output characteristics are recorded over the range $3 \lesssim N \lesssim 65$, with bistability observed for $N \gtrsim 15$ intracavity atoms and for a saturation photon number $n_0 \simeq 0.8$. For weak excitation the transmitted field exhibits photon antibunching as a nonclassical manifestation of state reduction and quantum interference with the magnitude of the nonclassical effects largely independent of N.

PACS numbers: 42.50.Kb, 32.80.−t, 42.50.Dv, 42.65.Pc

The dynamical processes for two-state atoms coupled to the electromagnetic field of a resonant cavity provide a paradigm for investigations of quantum dynamics in a dissipative setting [1,2]. Of particular interest is the prospect for studies in a regime of strong coupling such that the frequency scale g associated with reversible internal evolution is larger than the dissipative rate γ to an external environment. While a number of features related to structural aspects of the atom-cavity system have been observed (e.g., level shifts and linewidths) [2], unfortunately only a few experiments have been performed under conditions of strong coupling for which the critical number of quanta $(\gamma/g)^2$ which characterizes the system evolution is small [2-4]. In the domain $(\gamma/g)^2 < 1$, the usual system-size expansions of quantum statistical physics are not applicable; dynamical fluctuations at the level of a single photon or atom can have profound effects on the system's evolution even for large numbers of photons or atoms. Beyond the immediate relevance to quantum optics, investigations in cavity QED in a regime of strong coupling provide realizable avenues for the exploration of questions such as the scaling of quantum fluctuations with system size and the nature of global quantum correlations for open quantum systems [5].

Within this general context, the subject of this Letter is the quantum statistical behavior of N two-state atoms strongly coupled to a single mode of a high-finesse optical cavity. Of principal importance are the single-atom cooperativity parameter $C_1 \equiv g_0^2/2\kappa\gamma_\perp$ and the saturation photon number $n_0 \equiv (\gamma_\perp \gamma_\parallel / 4 g_0^2) b$, where κ is the decay rate of the cavity field, $\gamma_\parallel, \gamma_\perp$ are the decay rates of the atomic inversion and polarization into modes outside the cavity, g_0 is the optimum coupling rate of an atom to the field mode, and b depends on the cavity geometry. For our experiment $C_1 \simeq 2.3$ and $n_0 \simeq 0.8$, so that critical phenomena such as optical bistability are observed with a small number of atoms and only a few photons. To explore this behavior, we record the nonlinear input-output characteristics for the atom-cavity system over the range $3 \lesssim N \lesssim 65$ and make quantitative comparisons with the semiclassical theory based on the Maxwell-Bloch equations [1]. To address nonclassical aspects of the dynamics of this open quantum system, we investigate the intensity fluctuations of the intracavity field and observe both photon antibunching and sub-Poissonian photon statistics

[6,7] and interpret these results in terms of quantum state reduction and interference in a dissipative dynamical setting [7].

As illustrated in Fig. 1, our experiment consists of an optical cavity of finesse 8×10^4 formed by the two spherical mirrors (M_i, M_o) of radii 173 mm and approximate transmission coefficients $T_i \simeq 1 \times 10^{-5}$ and $T_o \simeq 4 \times 10^{-5}$. An optically pumped beam of cesium atoms (collimation $\pm 10^{-3}$ rad) intersects the cavity axis at approximately 90°, with the transition investigated being the $(6S_{1/2}, F=4, M_F=4) \rightarrow (6P_{3/2}, F'=5, M_F'=5)$ transition of the D_2 line of atomic Cs at 852 nm. Since the fraction of the total 4π solid angle subtended by our cavity is small $(\sim 10^{-5})$, $\gamma_\parallel^{-1}$ equals the free-space lifetime of 32 ns. Furthermore, since the coupling coefficient of an atom to the cavity mode is spatially dependent, we take $g(\mathbf{r}) \equiv g_0 \psi(\mathbf{r})$, where $g_0 \equiv (\mu^2 \omega_c / 2\hbar\epsilon_0 V)^{1/2}$ is the optimum coupling rate, $\psi(\mathbf{r})$ is the cavity-mode function normalized such that $\int |\psi(\mathbf{r})|^2 d^3 x = V$, and the effective atomic number $N \equiv \sum_i |\psi(\mathbf{r}_i)|^2$. Here μ is the transition dipole moment, ω_c is the frequency of the cavity resonance, $V = \pi w_0^2 l / 4$ is the mode volume, and $b = \frac{8}{3}$ is the geometric factor for our TEM$_{00}$ mode of waist $w_0 = 50$ μm and length $l = 1$ mm. We then have $[g_0, \gamma_\perp, \kappa] = [2\pi(3.2 \pm 0.2, 2.5 \pm 0.2, 0.9 \pm 0.1)]$ MHz, with each rate much larger than the inverse of the atomic transit time τ_t $(4 \times 10^{-7}$ s to traverse $2w_0)$. The signal beam which excites the system is provided by a titanium-sapphire laser of rms linewidth $\simeq 60$ kHz and is matched to the TEM$_{00}$ cavity mode. The cavity length is actively stabilized with a chopping technique that alternates between data collection (with detectors D2,D3) and stabilization (with detector D4) at a rate of 2.5 kHz with an acousto-optic modulator (AOM). For all measurements the cavity and atomic detunings are nearly zero (± 200
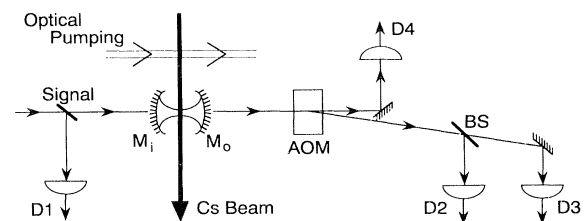
FIG. 1. Diagram of principal elements of the experiment.

kHz).

To investigate the steady-state operating characteristics of the atom-cavity system, we record the transmitted power P_t registered by the detector D3 as a function of input power P_i at the detector D1. The results for four atomic densities are shown in Fig. 2, which is a log-log plot of the intracavity intensity $X = 3P_t/\pi w_0^2 I_s T_o$ versus the input intensity $Y = 3P_i T/\pi w_0^2 I_s T_o$, where $I_s = 1$ mW/cm^2 and the empty-cavity peak transmission $T \simeq 0.25$. As studied in previous experiments in a regime of weak coupling [8], the semiclassical theory of optical bistability gives $Y = X[1 + 2C\chi(X)]^2$, where the atomic cooperativity parameter $C \equiv C_1 N$ and the susceptibility $\chi(X) = (3/2X)\ln[\frac{1}{2} + \frac{1}{2}(1 + 8X/3)^{1/2}]$ [8]. In Fig. 2 we plot $Y(X)$ averaged over the (assumed) Poisson fluctuations in N for each of the data sets. For each atomic density, we determine C and hence N by optimizing the fit of $Y(X)$ to the data on the upper and lower branches far from the turning points. Our measurements fix X in absolute terms within $\pm 10\%$; the recorded values of P_i are scaled into dimensionless intensities Y with a single fitting parameter for all the data.

While the agreement between the experiment and the semiclassical theory is reasonable away from the turning
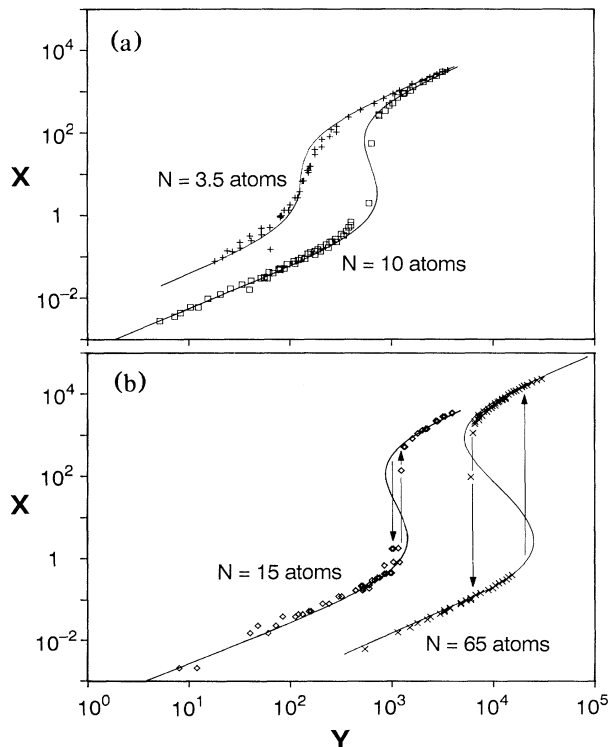
FIG. 2. Intracavity intensity X vs input intensity Y for four atomic densities corresponding to intracavity atomic numbers of (a) $N = 3.5$ and 10; (b) $N = 15$ and 65. Note that this is a log-log plot, with $X = 1$ corresponding to photon number $n_0 = 0.8$. The solid curves are from the semiclassical state equation as discussed in the text.

points, it is poor in the neighborhood of the hysteresis cycle with large dispersion observed for the values of the switching points in successive sweeps of Y with other external control parameters held constant. An obvious source for this dispersion and the discrepancies in the fits of Fig. 2 is the dynamic nature of the atomic-number fluctuations, which occur on a time scale given by τ_t. For example, fluctuations for which $N \rightarrow N - \Delta N$ ($N + \Delta N$) will cause premature passage from the lower (upper) to the upper (lower) branch and hence will erode the right (left) side of the hysteresis loop. Likewise, intrinsic quantum fluctuations of the atom-field interaction can lead to the loss of local stability of the semiclassical states and to quantum switching near the turning points [1,9]. As a result of these (and possibly other) microscopic fluctuations, the observed width of the bistability trace is considerably narrowed as indicated by the arrows in Fig. 2(b) which delineate the boundaries of the hysteresis cycle measured when Y is scanned at a slow rate (100 Hz). Whereas the semiclassical theory for $Y(X)$ predicts the critical onset of bistability for $C \simeq 10$ and $N \simeq 5$, in fact we observe bistability only for $C \gtrsim 30$ and $N \gtrsim 15$.

Turning now to our measurements of the photon statistics of the transmitted field, we employ the detectors D2,D3 shown in Fig. 1 to accumulate histograms of the number of coincidences $m(\tau)$ versus time delay τ. The detector D2 provides "start" pulses to a set of two time-to-digital converters (TDC) and is an actively quenched avalanche photodiode with quantum efficiency 28%. Detector D3 provides "stop" pulses and is a photomultiplier tube of quantum efficiency 7%. One TDC serves as the primary timing unit for a stop given a start, while a second unit detects infrequent second stop events. The counting rates of D2,D3 are continuously monitored with a typical counting rate at D2 being 30 kHz, which is a factor of 20 above the background level and which corresponds to $X = 0.05$. In Fig. 3 we present two raw histograms for $m(\tau)$ taken with $N = 18$ and 110. Time delay $\tau > 0$ (< 0) corresponds to a start event followed (preceded) by a stop event, with $\tau = 0$ referenced to simultaneous events at the beam splitter (BS) in Fig. 1 (as established with short pulses from a laser diode). The apparent activity around $\tau = 0$ and extending to times of about 0.1 μs is associated with the dynamics of the atom-cavity system, while for $\tau \geq 0.6$ μs, $m(\tau)$ settles to a level m_P associated with random coincidences from independent processes at D2,D3, with the Poisson level m_P separately determined and not fitted. Although $m(\tau)$ in Fig. 3(b) is relatively symmetric in its deviations about m_P, we find a broad excess above m_P in Fig. 3(a) for $|\tau| \lesssim 0.4$ μs resulting from fluctuations in the number of atoms inside the cavity. These fluctuations have a time scale given by the atomic transit time and stochastically modulate C and hence the transmitted field with an increasing fractional effect for decreasing N.

Focusing our attention now on the region near $\tau = 0$ in Fig. 3, we employ the ratio $m(\tau)/m_P$ to infer the intensi-
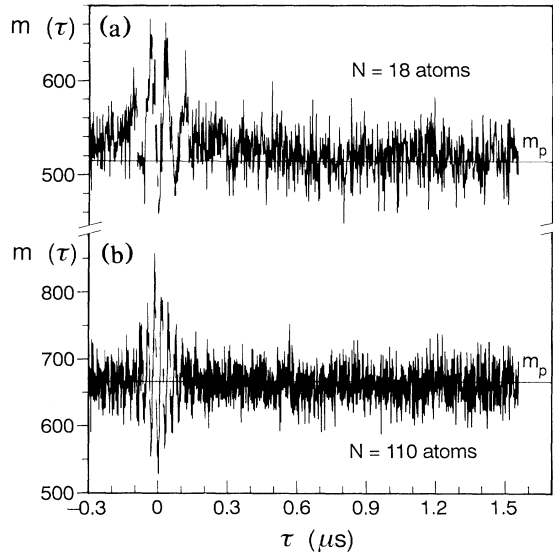
FIG. 3. Number of photoelectric coincidences $m(\tau)$ vs time delay τ, with the expected number of random coincidences m_P indicated. (a) $N=18$; (b) $N=110$.

FIG. 4. Intensity correlation function $g^{(2)}(\tau)$ vs time delay τ for (a)-(c) $N=18$, 45, and 110, respectively. The data in (a) and (c) are from Figs. 3(a) and 3(b), respectively, but are normalized to m_P and plotted with an expanded abscissa. In (a)-(c) a three-point smoothing algorithm has been applied. The solid curves are theoretical results as discussed in the text.

ty correlation function $g^{(2)}(\tau)=\langle:\hat{I}(t)\hat{I}(t+\tau):\rangle/\langle\hat{I}\rangle^2$ for the field intensity $\hat{I}$ transmitted by the cavity (the colons denote normal and time ordering). Results for $g^{(2)}(\tau)$ are shown in Fig. 4 for three atomic beam densities. Photon antibunching $[g^{(2)}(0)<g^{(2)}(\tau)]$ and sub-Poissonian photon statistics $[g^{(2)}(0)<1]$ are clearly observed for each of the traces in Fig. 4. These characteristics of the data are not allowed for a classical stochastic process and are indicative of the manifestly quantum nature of the dynamical processes of the atom-cavity system. In addition to the behavior near $\tau=0$, the data also exhibit an oscillatory regression for larger $|\tau|$ as determined by the system eigenvalues, which in the weak-field limit are $\lambda_\pm=-\beta\pm i\Omega$, where the damping rate $\beta=\frac{1}{2}(\kappa+\gamma_\perp)$ and the normal-mode splitting $\Omega=[g_0^2N-\frac{1}{4}(\kappa-\gamma_\perp)^2]^{1/2}$ [10]. From Lorentzian fits to Fourier transforms of the data sets in Fig. 4, we can determine β and Ω; the results for the data in 4(a)-4(c) are $\beta/2\pi=1.9$, 2.1, and 2.1 MHz and $\Omega/2\pi=13.7\pm0.4$, 21.3 ± 0.4, and 33.7 ± 0.4 MHz, respectively. Note that the values for $\beta/2\pi$ are below the natural half-width of 2.5 MHz as a result of linewidth averaging ($\kappa<\gamma_\perp$), but are not as small as $\frac{1}{2}(\kappa+\gamma_\perp)/2\pi=1.7$ MHz, principally due to transit broadening. Given g_0 from the cavity geometry and atomic parameters, we can extract the mean numbers N for each trace [4(a)-4(c)], with the results $N=18\pm3$, 45 ± 5, and 110 ± 14, which are in reasonable agreement with estimates from fits to the input-output characteristics as in Fig. 2.

Beyond these initial characterizations, we can attempt to obtain a detailed theoretical description of our data for $g^{(2)}(\tau)$ by generalizing the theory of Ref. [7] to the case

$g\to g(\mathbf{r})$. This approach yields

$$g^{(2)}(\tau)=\{1+(\Delta a/a)\exp(-\beta\tau)$$
$$\times[\cos\Omega\tau+(\beta/\Omega)\sin\Omega\tau]\}^2,$$

with

$$\frac{\Delta a}{a}=2C\frac{1-[(1+C')/C']\sum_i[C_i'/(1+C'-2C_i')]}{1+(1+\gamma_\parallel/\kappa)\sum_i[C_i'/(1+C'-2C_i')]}, \quad (1)$$

where $C_i=g(\mathbf{r}_i)^2/2\gamma_\perp\kappa$ and the primed quantities are the corresponding unprimed quantities divided by $1+\gamma_\perp/\kappa$. Our theoretical results for $g^{(2)}(\tau)$ are shown graphically in Fig. 4 by the solid curves, which match the experimental results quite well. In plotting these curves, the experimentally determined values of g_0, κ, and N have been used and a simulation employed for evaluating the summations in (1) with atoms placed randomly and repeatedly over a volume $V'\gg V$, where the average number of atoms in V is given by N. The caveat in our analysis is that we have scaled the theoretical results for $|g^{(2)}(0)$

$-1|$ down by a factor of 4 in 4(a)-4(c) and shifted the curves for 4(a) and 4(b) up slightly to account for the excess noise from fluctuations in N as discussed above. Apparently the transient nature of the atomic motion through the cavity mode (which is not included here or in Ref. [7]) has a profound effect in decorrelating the otherwise coherent response of the sample to the escape of a photon. Support for this conjecture comes from a weak-coupling theory (which is not directly applicable to our work), where homogeneous dephasing $\gamma_\perp \rightarrow 1.2\gamma_\perp$ leads to an approximate threefold reduction in $|g^{(2)}(0)-1|$ for parameters comparable to those in Fig. 4 [11]. Empirically, we also know that $|g^{(2)}(0)-1|$ is reduced somewhat because the weak-field limit is not strictly satisfied in our measurements.

To interpret these results, we note the close correspondence with Ref. [7]. The escape of a photon projects the atom-cavity wave function into a reduced state that can deviate significantly from the steady state if C_1 is large. Since there are multiple indistinguishable paths that can lead to the detection of two photons [7], the respective probability amplitudes must be summed and then squared, as reflected by the fact that the expression for $g^{(2)}(\tau)$ is a perfect square. That the intracavity field of the reduced state is smaller than that of the steady state [and hence $g^{(2)}(0) < 1$] results from this intrinsic indistinguishability together with the increase in the atomic polarization field near $\tau = 0$ by an amount of order C_1 due to the momentary loss of the reaction field from one atom in the cavity. However, in contrast to an intuition rooted in the standard weak-coupling theory of optical bistability [1], the quantum fluctuations of the system do not scale as $1/N$ for increasing number of atoms, as is clear from Fig. 4. The process whereby a single atom makes a transition to its ground state can have a profound consequence even for $N \gg 1$.

In summary, we have investigated the behavior of a strongly coupled atom-cavity system with measurements of both optical bistability and photon statistics. The discrepancies evidenced in Fig. 2 for the steady-state characteristics warrant further study particularly with regard to the question of global quantum correlations in a dissipative setting. Our observations of photon antibunching and sub-Poissonian photon statistics indicate a scaling for quantum fluctuations contrary to that for weakly coupled systems, with the functional form of $g^{(2)}(\tau)$ reflecting the underlying processes of state reduction and quantum interference for an open (dissipative) system in a nonperturbative regime. Finally, note that the nonclassical light is transmitted as a Guassian beam and is thus readily available as a source for various experiments in quantum optics.

[a]Present address: Max-Planck Institut für Quantenoptik, 8046 Garching, Germany.

[b]Present address: University of Texas, Austin, Texas 78712.

[1] L. A. Lugiato, in *Progress in Optics*, edited by E. Wolf (North-Holland, Amsterdam, 1984), Vol. 21, p. 71.

[2] E. A. Hinds, in *Advances in Atomic, Molecular and Optical Physics*, edited by D. Bates and B. Bederson (Academic, New York, 1990), Vol. 28, p. 237.

[3] G. Rempe *et al.*, Phys. Rev. Lett. **64**, 2783 (1990).

[4] M. Brune *et al.*, Phys. Rev. Lett. **59**, 1899 (1987).

[5] P. Meystre *et al.*, Opt. Commun. **79**, 300 (1990); C. M. Savage and H. J. Carmichael, IEEE J. Quantum Electron. **24**, 1495 (1988).

[6] F. Casagrande and L. A. Lugiato, Nuovo Cimento B **55**, 173 (1980); P. D. Drummond and D. F. Walls, J. Phys. A **13**, 725 (1980).

[7] H. J. Carmichael *et al.*, Opt. Commun. **82**, 73 (1991).

[8] A. T. Rosenberger *et al.*, Phys. Rev. A **43**, 6284 (1991).

[9] P. D. Drummond, Phys. Rev. A **33**, 4462 (1986).

[10] M. G. Raizen *et al.*, Phys. Rev. Lett. **63**, 240 (1989).

[11] R. J. Brecha, Ph.D. thesis, University of Texas, 1990 (unpublished).